Hard-template synthesis of titanium dioxide hollow spheres

Anna Kusior, Andrzej Warchal, Stanislaw Komornicki, Marta Radecka

Faculty of Materials Science and Ceramics, AGH University of Science and Technology, Krakow 30-059, Poland
E-mail: akusior@agh.edu.pl

Published in Micro & Nano Letters; Received on 8th July 2014; Revised on 5th September 2014; Accepted on 9th September 2014

An easy approach for the fabrication of titanium dioxide hollow spheres is proposed. Nanostructures were obtained by the conventional hard template method with silica-protected calcination. The samples were characterised by differential thermal analysis and thermogravimetry, Brunauer-Emmett-Teller nitrogen adsorption isotherms, X-ray diffraction, scanning and transmission electron microscopy (SEM and TEM). Raman spectroscopy and optical properties of the prepared materials were studied as well. X-ray analysis has shown that the silica protection layer allows direct phase transformation from amorphous titania to crystalline anatase regardless of the temperature. The crystallite size is more than 5 nm. The diameter of the obtained hollow nanostructures is within the range 115–420 nm. The thickness of the walls varies from 12 to 38 nm depending on annealing conditions. TEM and SEM images confirm their spherical shape.

1. Introduction: Zero-dimensional (0D) nanomaterials (three dimensions in the nanometric range) such as hollow spheres often exhibit physical and chemical properties different from those of polycrystalline materials. They can be characterised by higher specific surface area (SSA), reduced diffusion resistance, lower density and better permeation. All these parameters are suitable for highly active nanostructured catalysts and for many other purposes. Their design has attracted considerable attention because of their wide application in numerous fields like drug delivery, gas sensing materials [1] or lithium (Li)-ion batteries [2, 3]. Owing to their structure they enhance the light harvesting capabilities [4], which make them good materials for use in photocatalysis [5] and dye-sensitised solar cells [6].

There are several methods for the preparation of hollow sphere nanostructures [7]. The main division covers the conventional hard-template method, including layer-by-layer assembling [8] and templating against colloidal particles [9], where the shape and size of the obtained material are directly determined by the substrate, soft-template synthesis, where the basis is a liquid (emulsion droplets [10]) or gaseous (bubbles [11]) and methods without any seed, such as the inside-out Ostwald ripening process [12]. Preparation of hollow spheres using the hard template process consists typically of four steps: (i) template preparation, (ii) surface modification, (iii) coating templates and (iv) selective removal by calcination and/or by the dissolution of templates [7, 13, 14]. Colloidal silica particles [3] and the polymeric latex [5] can be used in most cases as seeds because of their availability in a wide range of sizes of monodispersive materials.

Titanium dioxide (TiO_2) is a wideband semiconductor suitable for photocatalysis, solar cells and Li-ion batteries [15–21]. It offers a number of advantages such as low cost, is non-toxic, and has high chemical and optical stability [22]. TiO_2 exists in three polymorphic forms: rutile, Brookite and anatase. The last structure is the most active phase in photocatalysis [23] because of the lowest charge recombination rate and higher reduction potential [22]. Important parameters of TiO_2 applications are crystallinity and SSA. The degree of crystallinity is an important factor in enhancing the generation of e^- and h^+ pairs, while a high SSA corresponds to the number of reaction sites (active centres). The annealing of material at higher temperatures results in an increase of the grain size with decreasing the SSA. Moreover, the phase transformation of TiO_2 occurs (anatase to rutile). To prevent this last process and the excessive outgrowth of the outer layer, silicon dioxide (SiO_2) is applied to its surface [13, 24–26]. The silica-protected calcination method allows changing the amorphous titania to the crystalline anatase form with a mesoporous characteristic and prevents cracking of the shell.

Chemical etching using sodium hydroxide (NaOH) solution removes the SiO_2 core and coating and enables the creation of mesoscale porosity because of the formation of small spaces between titania nanograins.

This Letter reports the preparation and characterisation of anatase-rich TiO_2 hollow spheres, where in contrast to the published papers [13, 24, 25] the first step of template preparation was eliminated using commercially available nanoscale fumed silica and a lower concentration of NaOH for etching.

2. Experimental

2.1. Preparation: Titania hollow spheres were prepared using the conventional template method with silica-protected calcination. As a substrate, commercial synthetic, amorphous fumed, high-purity SiO_2 (CABOT GmbH) was used. CAB-O-SIL®M-5 is an extremely fine particle size silica aerogel with an extremely large surface area, 200 m^2/g (D_{BET}-13, 63 nm). Owing to the substantial deployment of surface, grains are strongly aggregated. SiO_2 nanopowder was dispersed in a solution of hydroxypropyl cellulose (HPC, Sigma Aldrich) as a surfactant for adhesion promotion, ethanol (EtOH) and distilled water (DI water). After stirring for 30 min, a mixture of titanium isopropoxide (TIPP, Sigma Aldrich) and EtOH (proportion ratio 1:5) was added. The mixture was then heated to 80°C for 60 min. To obtain a thicker layer of TiO_2, this process was repeated three times.

Core–shell SiO_2@TiO_2 structures thus obtained were left for 24 h at room temperature in a solution of polivinylopropanol (PVP, MW ~40 000, Sigma Aldrich) and then covered with a protective layer of SiO_2 with tetraethyl ortosilicate (TEOS, Sigma Aldrich). The resulting nanostructures of SiO_2@TiO_2@SiO_2 were then annealed in air at 600°C or 850°C for 2 h. Samples were then etched with a 0.25 M NaOH (containing 3×10^{-4} M Na_2CO_3) solution for times of 2, 4 and 6 h at 80°C. The preparation procedure is presented in Fig. 1.

2.2. Characterisation: The structure of the obtained samples was studied by X-ray diffraction (XRD) in Bragg-Brentano (BB) and grazing incidence diffraction (GID) geometry with a Cu-Kα radiation source using an X'Pert MPD Philips diffractometer. Phases were identified using the ICDD database. The morphology studies were carried out with a JEOL 5400 scanning electron microscope (SEM) equipped with an EDS analyser and with a

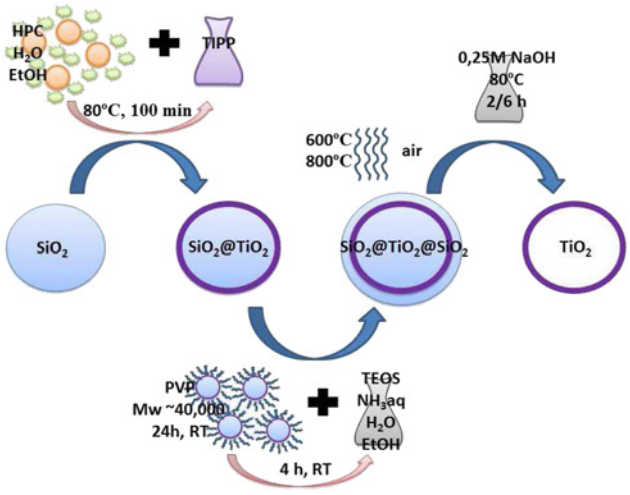

Figure 1 *Preparation of TiO_2 nanostructures (hollow spheres)*

JEOL-JEM1011 transmission electron microscope (TEM). The SSA was determined by Brunauer-Emmett-Teller (BET) nitrogen adsorption isotherms with Nova 1200e, Quantachrome. The Raman spectra of the powders were recorded using a Jobin-Yvon LabRam HR800 spectrometer equipped with a confocal Olympus microscope and a 100× objective. The incident laser excitation was provided by a 532 nm laser. Spectra were recorded in the range of 100–1000 cm^{-1}. An 800 g/mm diffraction grating was used. Optical properties were studied over a wide wavelength range of 250–2500 nm with a Lambda 19 Perkin-Elmer double-beam spectrophotometer equipped with a 150 mm integrating sphere. The results for the commercial P25 nanopowder, well known for its photocatalytic properties, are included for comparison. Mixed rutile/anatase phase (20%/80%) P25 is characterised by SSA 50 m^2/g and by an average primary particle size of 21 nm [27]. Differential thermal analysis and thermogravimetry (DTA/TG), measurements were recorded using Instruments' SDT 2960 TA apparatus in the temperature range of 30–990°C. The nanopowder samples were placed in standard platinum crucibles and heated at a rate of 10°C/min in synthetic air atmospheres under a flow of 100 cm^3/min. Volatile products of decomposition were analysed by a quadrupole mass spectrometer ThermoStar QMS 300 Blazers, connected online to the SDT 2960 system.

3. Results and discussion: TG measurements of the SiO_2 template and $SiO_2@TiO_2@SiO_2$ powder after reaction and the DTA and mass spectrometry data of (STS1) are presented in Fig. 2. The loss of mass during heating is higher for STS1 than for the silica template, 24 and 1.8%, respectively. Following the analysis of the DTA curve together with the mass spectrometer signals for SiO_2 (not presented in Fig. 2), one can conclude that the mass loss is related to dehydration. Thermal decomposition of as-prepared nanopowder proceeds through some overlapping stages. The first step occurs between 35 and 90°C and it is described by a small endothermic effect on the DTA curve. The analysis of gaseous products by the mass spectrometer indicates at this stage the presence of water, which seems to be absorbed by the material. In the second step, a strong exothermic effect can be observed from the temperature of 200°C together with a large amount of CO_2 and H_2O. Signals related to hydrocarbon chains ($m/z = 26$, 30, 38–41 and 43 – not shown in Fig. 2) are also present. This indicates that the decomposition and combustion process of some organic residues resulting from synthesis occurs. On the basis of data obtained from the DTA/TG powder analyses two annealing temperatures of 600 and 850°C were proposed. The first of them was selected due to the fact that the organic compounds used in

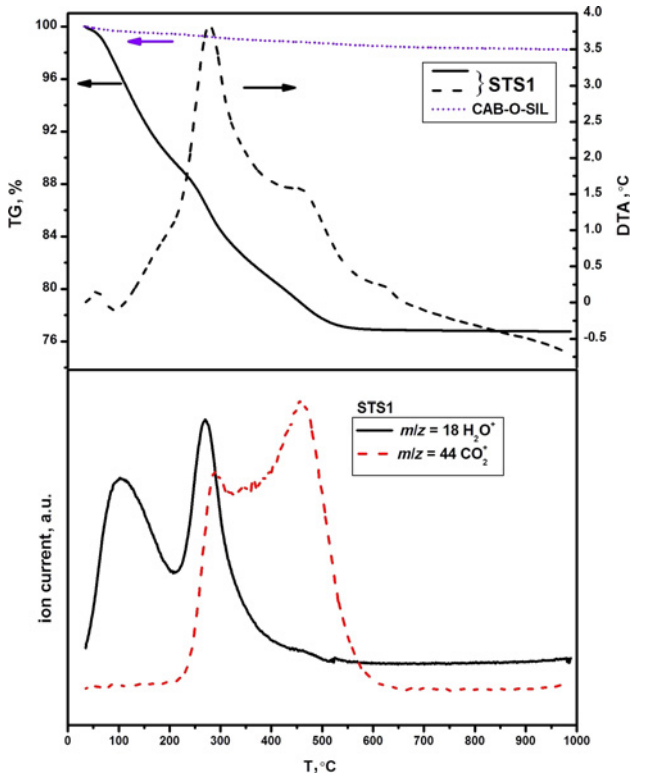

Figure 2 *Thermal decomposition data for STS1 and CAB-O-SIL with mass spectrometry analysis of gaseous products of decomposition*

the preparation of powders are completely decomposed, and the second is to verify if the protective layer of silicon dioxide prevents the growth of grains, and thereby the transformation of the TiO_2 structure from anatase to rutile.

3.1. Structure and morphology: Table 1 shows the data related to chemical composition, annealing temperature, etching time and crystallite size.

Diffraction patterns recorded in the GID geometry of TiO_2-based nanostructures as-prepared and annealed at 600°C are presented in Fig. 3. The phase analysis of the X-ray data reveals that all samples are crystallised in the anatase structure. During the etching process reaction of titania leads to the creation of sodium titanate species [24]. The as-formed Si–O–Ti bonds break and convert to sodium titanate in the presence of NaOH. After etching in NaOH for 2 h, monoclinic sodium carbonate (Na_2CO_3) appears. It can be concluded that the formed Ti–O–Na bond is broken and reaction with CO_2 (or Na_2CO_3) dissolved in DI water or contained in air can occur. Data have also shown that not all silica is removed, after calcination fumed CAB-O-SIL crystallised in the monoclinic coesite phase. The 4 h etching process allows removal of most of the Na_2CO_3 from the samples. The obtained nanopowder contains

Table 1 Chemical composition of prepared TiO_2-based nanostructures

Symbol	Chemical composition	Annealing temperature, °C	Etching time, h	Crystallite size, nm
STS1	$SiO_2@TiO_2@SiO_2$	–	–	–
STS2	$SiO_2@TiO_2@SiO_2$	600	–	5
STS3	TiO_2	600	2	5
STS4	TiO_2	600	4	5
STS5	$SiO_2@TiO_2@SiO_2$	850	–	7
STS6	TiO_2	850	6	7

doi: 10.1049/mnl.2014.0414

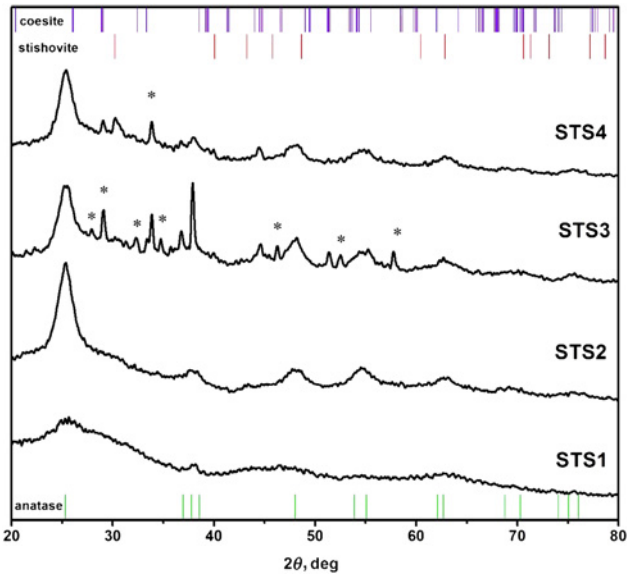

Figure 3 *XRD patterns in GID geometry, * corresponds to Na_2CO_3*

less foreign phases. Moreover, the crystallite size, calculated from the Scherrer formula [28], remains unchanged and is ca. 5 nm for all samples (Table 1). The minor amount of SiO_2 occurs in tetragonal stishovite form. To verify that there are no additional species on the surface, comparative X-ray analysis in both configurations, BB and GID, were carried out for all samples. There were no differences. The XRD study of the sample annealed at 850°C and etched for 6 h in NaOH comparing these methods is shown in Fig. 4. Phase analysis of the diffraction data has shown that Na_2CO_3 is still present, and the silica was not totally removed. For all the samples silica-protected calcination delays the transformation from amorphous TiO_2 to crystalline anatase; this behaviour is independent of thermal treatment. Moreover, there was no overgrowth observed, the calculated crystallite size of the prepared samples is slightly changed, from 5 to 7 nm (Table 1). Despite the use of high temperature, an anatase structure was achieved, which is consistent with reports on the influence of a protective silica layer and the specificity of the polymorphic transformation of nanoTiO_2 [29–31].

The Raman spectra for all samples are presented in Fig. 5. For the as-prepared powder STS1, broad peaks of anatase [32, 33] (154 and 637 cm^{-1}) and SiO_2 [34] (274 and 520 cm^{-1}) were initially

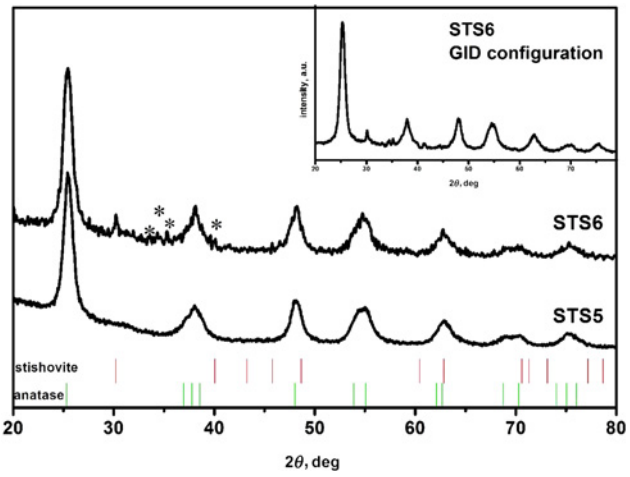

Figure 4 *XRD patterns in BB geometry for a sample annealed at 850°C before (STS5) and after (STS6) etching for 6 h in NaOH; inner data contains comparative data in GID configuration, * corresponds to Na_2CO_3 reflexes*

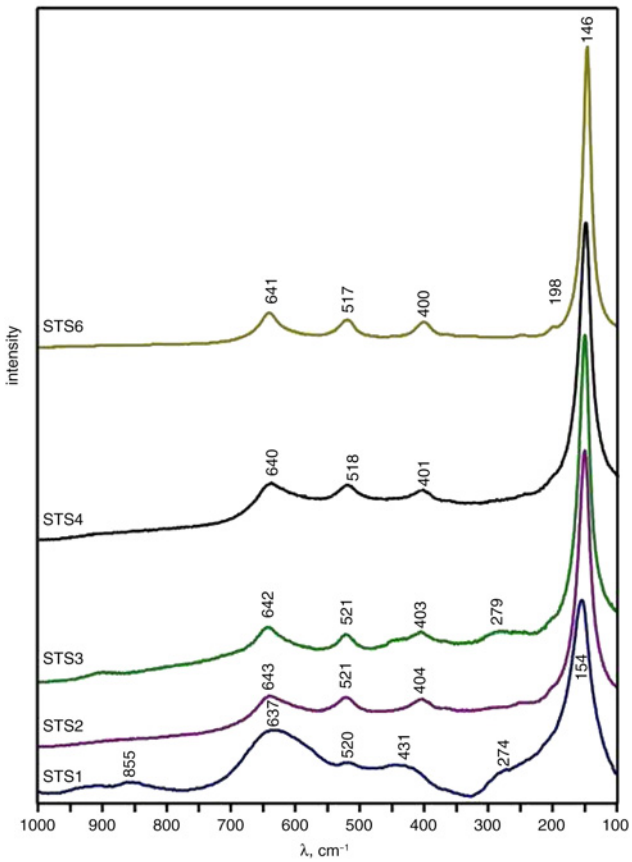

Figure 5 *Raman spectra of TiO_2-based nanostructures*

observed. Annealing in air at 600 and 850°C results in the formation of anatase as a dominant crystalline phase. The observed bands near 640, 517 and 400 cm^{-1} correspond to a disordered TiO_6^{8-} octahedron in anatase. The strongest mode at 144 cm^{-1} is related to external vibration of O–Ti–O band bending [35]. For the as-prepared sample rich in organic compounds, a broad peak in relation with C–C bonding in stretching mode near 855 cm^{-1} appears [36].

Fig. 6 presents the SEM images of different samples completed with EDS analysis and SSA data. One can observe that because of the relatively fine grains the SiO_2 template consists of spherical aggregates (Fig. 6*a*). This shape is typical for all obtained samples with the TiO_2 layer, and only slight changes in grain diameter are observed (Figs. 6*b–d*).

The EDS data for STS4 and STS6 confirm the presence of the Na-containing species in the samples. The value of the SSA is decreasing with increasing annealing temperature from 208 m^2/g for as-prepared SiO_2@TiO_2@SiO_2 powder to 27 m^2/g for the well-crystallised titania nanostructures.

The TEM images of the prepared TiO_2 hollow spheres are presented in the insets in Figs. 6*c* and *d*. It can be seen that etching in NaOH in some cases disrupts the continuity of the sphere, leading to the formation of cracks, but the spherical shape remains unchanged. The average wall thickness increases with calcination temperature while SSA decreases (cf. Table 2). These values are a few times higher than those for silica grains. The silica aggregates were the templates for TiO_2 precursor deposition.

3.2. Optical properties: Diffuse reflectance R_{Diff} as a function of the wavelength, typical for highly scattering samples, is shown in Fig. 7.

The fundamental absorption edge, which is characterised by an abrupt decrease in the diffuse reflectance when the photon energy approaches the value of the bandgap energy, E_g, occurs at higher

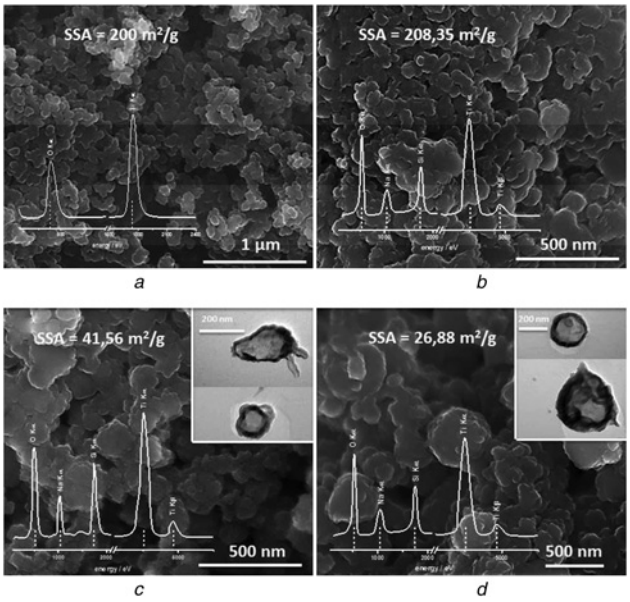

Figure 6 *SEM and TEM images of SiO_2 substrate, as-synthesised powder STS1, STS4, and STS6*
a SiO_2 substrate
b As-synthesised powder STS1
c STS4
d STS6

photon energies, $h\nu$, for the as-prepared sample than for the sample annealed at 600 and 850°C. The results of the application of the two methods of analysis of the diffuse reflectance spectra are presented.

On the basis of the derivative of the optical diffused reflectance spectra, $D_{\mathrm{Rdiff}} = \mathrm{d}R_{\mathrm{Diff}}/\mathrm{d}\lambda$, one can determine the energies of optical transitions, which correspond to the wavelength related to the maximum of the D_{Rdiff} curve. The inset in Fig. 7 demonstrates exemplary fitted curves D_{Rdiff} for the selected materials (ST1, ST6). The bandgap energy E_g was determined as well from the appropriate fits of the Kubelka-Munk (K-M) function and calculated directly from the diffuse reflectance spectra (Fig. 8). The calculations were performed according to (1). For nanopowders, we have used the K-M approach with the K-M function $K–M(R_\infty)$ defined as [37]

$$K - M(R_\infty) = (1 - R_\infty)^2/2R_\infty = k/s \qquad (1)$$

where R_∞ is the absolute reflectance of the sample, k is related to absorption, while s is because of the scattering. Assuming that the scattering is the same over a small wavelength region, the $K–M(R_\infty)$ function follows the changes in the absorption coefficient. Therefore, the appropriate fits of $(K–Mh\nu)^{1/n}$ against photon energy $h\nu$ can be used to determine E_g. The power coefficient n takes values of 1/2, 3/2, 2 or 3 depending on the type of transition: direct allowed, direct forbidden, indirect allowed or indirect forbidden, respectively.

Table 2 Dimensions of TiO_2-based nanostructures (calculated from TEM and BET)

Symbol	SSA, m^2/g	Sphere diameter, nm	Wall thickness, nm
STS1	208.35	–	–
STS3	69.37	115–310	13–25
STS4	41.56	120–320	12–23
STS5	50.42	–	–
STS6	26.88	180–390	23–38

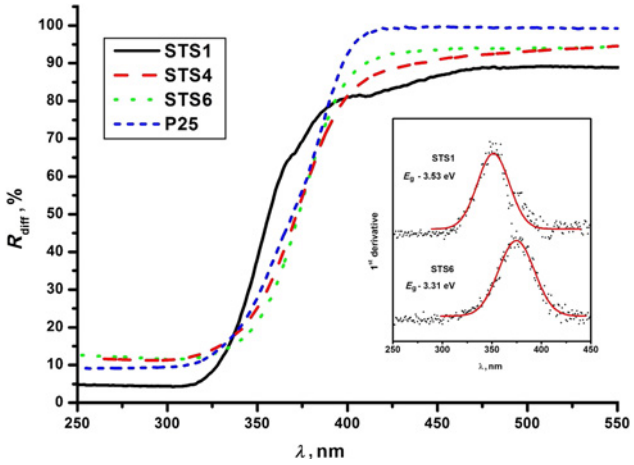

Figure 7 *Reflectance spectra of TiO_2-based nanostructures*
Result for commercial nanopowder P25 is given as a reference

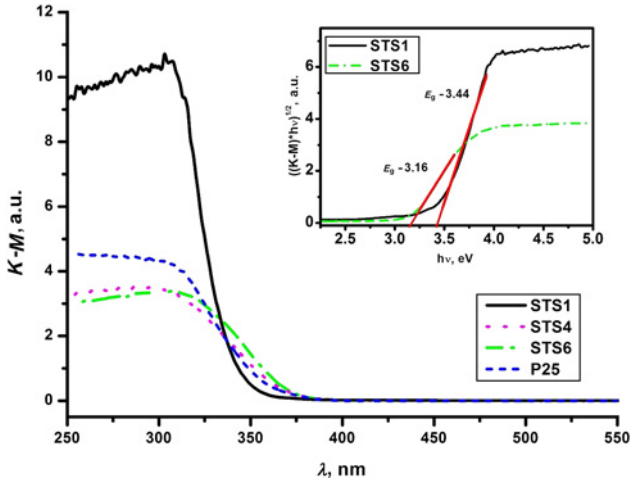

Figure 8 *K-M function and the Tauc plot of TiO_2-based nanostructures as a function of photon energy hv calculated for the power coefficient n = 2*

The experimental and theoretical data indicate two major optical transitions for TiO_2: indirect allowed and direct allowed with higher energy levels [38, 39]. The values of the calculated optical transition energies are given in Table 3. The E_g values obtained from both types of fits of the K-M function have the same trend as the R_{diff} spectra. The significant difference between direct allowed and indirect allowed transition also was observed. Comparison of the values of photon energies determined from the methods based

Table 3 Bandgap energy values of TiO_2-based nanostructures

Sample	Bandgap energy E_g, eV (±0.05 eV)		
	Indirect-allowed transition ($n = 2$)	Direct-allowed transition ($n = 1/2$)	Differential relation $\mathrm{d}R_{\mathrm{diff}}/\mathrm{d}\lambda$
STS1	3.44	3.73	3.53
STS4	3.12	3.53	3.33
STS5	3.09	3.36	3.21
STS6	3.16	3.47	3.31
P25			
anatase	3.3	3.68	3.42
rutile	3.1	3.54	3.18

doi: 10.1049/mnl.2014.0414

on the maximum of the first derivative of the diffuse reflectance or $(K–Mhv)^{1/2}$ indicates that there is not much difference between them. The observed decrease in the E_g value from about 3.44–3.53 eV to 3.16–3.31 eV corresponds to the evolutions of the structure. This is probably related to the crystalline anatase structure for the heat-treated hollow-sphere and the high contribution from the amorphous background in the case of the amorphous TiO_2 (STS1).

4. Conclusion: Anatase-phase TiO_2 hollow spheres were obtained using the hard-template method with silica-protected calcination. The commercial fused silica was used as a template. Samples were then characterised by means of XRD, Raman spectroscopy, electron microscopy SEM/TEM and optical spectrophotometry. The effect of bandgap energy E_g decreasing with annealing temperature was discussed. It has been shown that silica-protected calcination allows the control of the crystallinity and phase stability for TiO_2.

5. Acknowledgments: This project was financed by the National Science Centre (NCN) based on the decision number DEC-2012/07/B/ST8/03879. A. Kusior was partly supported by 'DOCTUS-Malopolski Fundusz Stypendialny dla Doktorantow'. S. Komornicki acknowledges the support of Statutory Project for Science for 2014 (no. 11.11.160.438).

6 References

[1] Yang G., Hu P., Cao Y., Yuan F.: 'Fabrication of porous TiO_2 hollow spheres and their application in gas sensing', *Nanoscale Res. Lett.*, 2010, **5**, pp. 1437–1441

[2] Chen J.S., Luan D., Li C.M., Boey F.Y.C., Qiao S., Lou X.W.: 'TiO_2 and SnO_2@TiO_2 hollow spheres assembled from anatase TiO_2 nanosheets with enhanced lithium storage properties', *Chem. Commun.*, 2010, **46**, pp. 8252–8254

[3] Liu J., Xue D.: 'Hollow nanostructured anode materials for Li-ion batteries', *Nanoscale Res. Lett.*, 2010, **5**, pp. 1525–1534

[4] Park J.H., Jung S.Y., Kim R., Park N.-G., Kim J., Lee S.-S.: 'Nanostructured photoelectrode consisting of TiO_2 hollow spheres for non-volatile electrolyte-based dye-sensitized solar cells', *J. Power Sources*, 2009, **194**, pp. 574–579

[5] Song C., Yu W., Zhao B., *ET AL.*: 'Efficient fabrication and photcatalytic properties of TiO_2 hollow spheres', *Catal Commun.*, 2009, **10**, pp. 650–654

[6] Koo H.J., Kim Y.J., Lee Y.H., Lee W.I., Kim K., Park N.-G.: 'Nano-embossed hollow spherical TiO_2 as bifunctional material for high-efficiency dye-sensitized solar cells', *Adv. Mater.*, 2008, **20**, pp. 195–199

[7] Lou X.W., Archer L.A., Yang Z.: 'Hollow micro-/nanostructures: synthesis and application', *Adv. Mater.*, 2008, **20**, pp. 3987–4019

[8] Caruso F.: 'Nanoengineering of inorganic and hybrid hollow spheres by colloidal templating', *Science*, 1998, **282**, pp. 1111–1114

[9] Zhong Z., Yin Y., gates B., Xia Y.: 'Preparation of mesoscale hollow spheres of TiO_2 and SnO_2 by templating against crystalline arrays of polystyrene beads', *Adv. Mater.*, 2000, **12**, pp. 206–209

[10] Collins A.M., Spickermann C., Mann S.: 'Synthesis of titania hollow microspheres by non-aqueous emulsion', *J. Mater. Chem.*, 2003, **13**, pp. 1112–1114

[11] Han Y., Fuji M., Shchukin D., Mohwald H., Takahashi M.: 'A new model for the synthesis of hollow particles via the bubble templating method', *Cryst. Growth Des.*, 2009, **9**, pp. 3771–3775

[12] Zeng H.C.: 'Ostwald ripening: a synthetic approach for hollow nanomaterials', *Curr. Nanosci.*, 2007, **3**, pp. 177–181

[13] Joo J.B., Zhang Q., Lee I., Dahl M., Zaera F., Yin Y.: 'Mesoporous anatase titania hollow spheres nanostructures though silica-protected calicnation', *Adv. Funct. Mater.*, 2012, **22**, pp. 166–174

[14] Zhang L., Fan T., Jiu H.: 'Fabrication and characterisation of hollow carbon/anatase titania', *Micro Nano Lett.*, 2010, **5**, pp. 351–354

[15] Nakata K., Fujishima A.: 'TiO_2 photocatalysis: design and application', *J. Photochem. Photobiol. C*, 2012, **13**, pp. 169–189

[16] Zhu C., Xia X., Liu J., *ET AL.*: 'TiO_2 nanotube @ SnO_2 nanoflake core-branch arrays for lithium-ion battery anode', *Nano Energy*, 2014, **4**, pp. 105–112

[17] Maira A.J., Yeung K.L., Soria J., *ET AL.*: 'Gas-phase photo-oxidation of toluene using nanometer-size TiO_2 catalysts', *Appl. Catal. B, Environ.*, 2001, **29**, pp. 327–336

[18] Lyson-Sypien B., Czapla A., Lubecka M., *ET AL.*: 'Gas sensing properties of TiO_2-SnO_2 nanomaterials', *Sens. Actuators B, Chem.*, 2013, **187**, pp. 445–454

[19] Radecka M., Rekas M., Trenczek-Zajac A., Zakrzewska K.: 'Importance of the band gap energy and flat band potential for application of modified TiO_2 photoanodes in water photolysis', *J. Power Sources*, 2008, **181**, pp. 46–55

[20] Kusior A., Klich-Kafel J., Trenczek-Zajac A., Swierczek K., Radecka M., Zakrzewska K.: 'TiO_2-SnO_2 nanomaterials for gas sensing and photocatalysis', *J. Eur. Ceram. Soc.*, 2013, **33**, pp. 2285–2290

[21] Zakrzewska K., Radecka M.: 'TiO_2-SnO_2 system for gas sensing – photodegradation of organic contaminants', *Thin Solid Films*, 2007, **515**, pp. 8332–8338

[22] Chen X., Mao S.S.: 'Titanium dioxide nanomaterials: synthesis, properties, modification and application', *Chem. Rev.*, 2007, **107**, pp. 2891–2959

[23] Luttrel T., Halpegamage S., Tao J., Kramer A., Sutter E., Batzill M.: 'Why is anatase a better photocatalyst than rutile? – model studies on epitaxial TiO_2 films', *Scientific Rep.*, 2014, **4**, pp. 1–8

[24] Zhang Z., Zhou Y., Zhang Y., *ET AL.*: 'Well-crystallized mesoporous TiO_2 shells for enhanced photocatalytic activity: prepared by carbon coating and silica-protected calcination', *Dalton Trans.*, 2013, **42**, pp. 5004–5012

[25] Joo J.B., Dahl M., Li N., Zaera F., Yin Y.: 'Tailored synthesis of mesoporous TiO_2 hollow nanostructures for catalytic applications', *Energy Environ. Sci.*, 2013, **6**, pp. 2082–2092

[26] United States Patent Number 4,075,031; Alvin Allen. assignor to E.I du Pont de Nemours and Company: 'TiO_2 pigment coated with dense silica and porous alumina/silica', Wilmington, Del., 1978

[27] AEROXIDE®TiO_2 P25, Evonik Industries, Product Information, https://www.aerosil.com/lpa-productfinder/page/productsbytext/detail.html?pid=1822

[28] Patterson A.L.: 'The Scherrer formula for *x*-ray particle size determination', *Phys. Rev.*, 1939, **56**, pp. 978–982

[29] Dahl M., Dang S., Joo J.B., Zhang Q., Yin Y.: 'Control of the crystallinity in TiO_2 microspheres through silica impregnation', *Cryst. Eng. Commun.*, 2012, **14**, pp. 7680–7685

[30] Gilbert B., Zhang H., Huang F., Finnegan M.P., Waychunas G.A., Banfield J.F.: 'Special phase transformation and crystal growth pathways observed in nanoparticles', *Geochem. Trans.*, 2003, **4**, (4), pp. 20–27

[31] Zhang H., Banfield J.F.: 'Understanding polymorphic phase transformation behavior during growth of nanocrystalline aggregates: insights from TiO_2', *J. Phys. Chem. B*, 2000, **104**, (15), pp. 3481–3487

[32] Ma W., Lu Z., Zhang M.: 'Investigation of structural transformation in nanophase titanium dioxide by Raman spectroscopy', *Appl. Phys. A*, 1998, **66**, pp. 621–627

[33] Frank O., Zukalova M., Laskova B., Kürti J., Koltai J., Kavan L.: 'Raman spectra of titanium dioxide (anatase, rutile) with identified oxygen isotopes (16, 17, 18)', *Phys. Chem. Chem. Phys.*, 2012, **14**, pp. 14567–14572

[34] Handbook of Minerals Raman Spectra, http://www.ens-lyon.fr/LST/Raman/index.php

[35] Ohsaka T., Izumi F., Fujiki Y.: 'Raman spectrum of anatase, TiO_2', *J. Raman Spectrosc.*, 1978, **7**, pp. 321–324

[36] Huang Z., McWilliams A., Lui H., McLean D.I., Lam S., Zeng H.: 'Near-infrared Raman spectroscopy for optical diagnosis of lung cancer', *Int. J. Cancer*, 2003, **107**, pp. 1047–1052

[37] Kubelka P.: 'New contribution to the optics of intensely light-scattering materials. Part I', *J. Opt. Soc. Am.*, 1948, **38**, pp. 448–457

[38] Tang H., Berger H., Schmid P.E., Levy F.: 'Optical properties of anatase (TiO_2)', *Solid State Commun.*, 1994, **92**, pp. 267–271

[39] Tang H., Prasad K., Sanjines R., Schmid P.E., Levy F.: 'Electrical and optical properties of TiO_2 anatase thin films', *J. Appl. Phys.*, 1994, **75**, pp. 2042–2047